e^+e^- pair production from γA reactions

M. Effenberger, E. L. Bratkovskaya, and U. Mosel
Institut für Theoretische Physik, Universität Giessen, D-35392 Giessen, Germany
(Received 10 March 1999; published 9 September 1999)

We present a calculation of e^+e^- production in γA reactions at MAMI and TJNAF energies within a semiclassical Boltzmann-Uehling-Uhlenbeck transport model. Dilepton invariant mass spectra for γC, γCa, and γPb are calculated at 0.8, 1.5, and 2.2 GeV. We focus on observable effects of medium modifications of the ρ and ω mesons. The in-medium widths of these mesons are taken into account in a dynamical, consistent way. We discuss the transport theoretical treatment of broad resonances. [S0556-2813(99)05609-5]

PACS number(s): 25.20.Lj, 13.60.Le, 14.40.Cs, 24.10.−i

I. INTRODUCTION

In-medium properties of hadrons are of fundamental interest with respect to an understanding of QCD in the nonperturbative regime (cf. [1]). During the past decade especially the properties of vector mesons have found widespread attention as they may be related to chiral symmetry [2–4].

A comparison of experimental data on dilepton production in nucleus-nucleus collisions at SPS energies [5,6] with transport theoretical calculations [7,8] seems to indicate a lowering of the ρ-meson mass in the nuclear medium. However, since in a heavy-ion collision the final dilepton yield is obtained by an integration over dileptons emitted at different densities and temperatures, a discrimination between different scenarios of in-medium modifications for the vector mesons is difficult [9,10].

Moreover, there is a more fundamental concern: ultrarelativistic heavy-ion reactions proceed, at least in their initial stages, far from equilibrium, whereas all theoretical predictions of in-medium properties are based on equilibrium assumptions. Therefore it is necessary to probe in-medium properties of vector mesons under ''cleaner'' conditions. For that purpose photon or pion induced reactions are promising tools. In such reactions the nuclear medium is very close to equilibrium at normal nuclear density and temperature zero. The predicted in-medium effects for the vector mesons are so large that they should have observable consequences already for densities $\rho=\rho_0$. Here one should note that even the dileptons seen in ultrarelativistic heavy ion reactions stem to a large part from densities $\rho\leqslant 2\rho_0$.

Our calculations are based on a semiclassical Boltzmann-Uehling-Uhlenbeck (BUU) transport model that has recently been very successfully applied to the description of heavy-ion collisions at SIS energies [11] and photoproduction of pions and etas in nuclei [12]. Meanwhile, we have extended the model to the description of dilepton as well as strangeness production and to the high energy regime by including the Lund string fragmentation model FRITIOF [13]. This allows us to calculate inclusive particle production in heavy ion collisions from 200*A* MeV to 200*A* GeV, in photon and pion induced reactions with the very same physical input. In our opinion, the simultaneous description of as many experimental observables as possible is necessary because of the large number of parameters, like unknown cross sections, and the strong assumptions that enter semiclassical transport models. In heavy-ion collisions particle production depends not only on a large number of elementary reaction channels but also on the global space-time evolution of the system. On the other hand, photon, pion, or proton induced reactions allow one to fix certain ingredients of the transport model as observables depend in general only on a few reaction channels. In Ref. [14] we have, for example, determined the in-medium η-nucleon cross section from photoproduction of Δ η mesons. Just recently we were able to improve considerably our treatment of the Δ resonance by comparing our calculations to experimental data on the photoproduction of pions [15].

Within our model we have already given predictions for dilepton production in pion nucleus reactions [16] that will be measured by the HADES Collaboration at GSI [17]. In the present paper we want to look at e^+e^- production in photonuclear reactions in the energy range from 0.8 to 2.2 GeV, which will be accessible at TJNAF [18] and at its lowest energy also at MAMI.

Our paper is organized as follows: In Sec. II we describe our model. Here we focus on the treatment of broad resonances and our description of elementary photon nucleon reactions. In Sec. III we present our results for dilepton production in photon nucleus reactions and discuss the possibility of subtracting the Bethe-Heitler contribution. In Sec. IV we include in-medium modifications for the vector mesons into our calculations and present their effect on the dilepton yield. We close with a summary in Sec. V.

II. BUU MODEL

The transport model used here has been developed starting from the model that has been described in full detail in Refs. [11,19]. Here we restrict ourselves to the description of the essential new features of our method.

A. Resonance properties

Instead of the baryonic resonances in Ref. [11] that were taken with their parameters from the PDG [20] we now use the resonances from the analysis of Manley and Saleski [21]. This has the advantage of supplying us with a consistent set of resonances. In particular, now the resonance parameters are consistent with the parametrizations of the resonance

widths. We take into account all resonances that are rated with at least two stars in Ref. [21]: $P_{33}(1232)$, $P_{11}(1440)$, $D_{13}(1520)$, $S_{11}(1535)$, $P_{33}(1600)$, $S_{31}(1620)$, $S_{11}(1650)$, $D_{15}(1675)$, $F_{15}(1680)$, $P_{13}(1879)$, $S_{31}(1900)$, $F_{35}(1905)$, $P_{31}(1910)$, $D_{35}(1930)$, $F_{37}(1950)$, $F_{17}(1990)$, $G_{17}(2190)$, and $D_{35}(2350)$. The resonances couple to the following channels: $N\pi$, $N\eta$, $N\omega$, ΛK, $\Delta(1232)\pi$, $N\rho$, $N\sigma$, $N(1440)\pi$, and $\Delta(1232)\rho$. The cross section for the production of a resonance R in a collision of a meson m with a baryon B is given by

$$\sigma_{mB\to R}=\frac{2J_R+1}{(2J_m+1)(2J_B+1)}\,\frac{4\pi}{k^2}\,\frac{s\Gamma^{\rm in}_{mB}\Gamma^{\rm out}_{\rm tot}}{(s-M_R^2)^2+s\Gamma^{\rm out2}_{\rm tot}}, \tag{1}$$

where J_R, J_m, and J_B denote the spins of the resonance, the baryon, and the meson, respectively. k is the c.m. system (c.m.s.) momentum of the incoming particles, s is the squared invariant energy, and M_R is the pole mass of the resonance. The total decay width $\Gamma^{\rm out}_{\rm tot}$ is given as a sum over the partial decay widths of the resonance. For a specific channel mB it is

$$\Gamma^{\rm out}_{mB}=\Gamma^0_{mB}\frac{\rho_{mB}(s)}{\rho_{mB}(M_R)}, \tag{2}$$

with Γ^0_{mB} being the partial decay width at the pole of the resonance and $\rho_{mB}(s)$ is given as

$$\rho_{mB}(s)=\int d\mu_m d\mu_B \mathcal{A}_m(\mu_m)\mathcal{A}_B(\mu_B) \times\frac{q(s,\mu_m,\mu_B)}{\sqrt{s}}B^2_{l_{mB}}(qR), \tag{3}$$

where $\mathcal{A}_m$ and $\mathcal{A}_B$ denote the spectral functions of the outgoing particles. q is their c.m.s. momentum, l_{mB} is their relative orbital angular momentum, and $B_{l_{mB}}$ is a Blatt-Weisskopf barrier penetration factor [22,21] (interaction radius $R=1$ fm). For the spectral function $\mathcal{A}_i$ of an unstable particle i we use

$$\mathcal{A}_i(\mu)=\frac{2}{\pi}\,\frac{\mu^2\Gamma_{\rm tot}(\mu)}{(\mu^2-M_i^2)^2+\mu^2\Gamma^2_{\rm tot}(\mu)}, \tag{4}$$

where M_i denotes the pole mass and $\Gamma_{\rm tot}(\mu)$ is the total width. Here we neglect any spin degrees of freedom as well as a momentum dependence of the real part of the self-energy. For a stable particle (with respect to the strong interaction) we simply have

$$\mathcal{A}_i(\mu)=\delta(\mu-M_i). \tag{5}$$

The incoming width $\Gamma^{\rm in}_{mB}$ in Eq. (1) is given by

$$\Gamma^{\rm in}_{mB}=C^{I_R}_{mB}\Gamma^0_{mB}\frac{kB^2_{l_{mB}}(kR)}{\sqrt{s}\rho_{mB}(M_R)}, \tag{6}$$

TABLE I. Properties of mesonic resonances. M_0 and Γ_0 denote the pole mass and the width at the pole mass, respectively.

Meson	M_0 [MeV]	Γ_0 [MeV]	Decay channels
ρ	770	151	$\pi\pi$
ω	782	8.4	$\pi\pi$ (2%), $\pi^0\gamma$ (9%), $\pi^+\pi^-\pi^0$ (89%)
ϕ	1020	4.4	$\rho\pi$ (13%), $K\bar{K}$ (84%), $\pi^+\pi^-\pi^0$ (3%)
σ	800	800	$\pi\pi$

where $C^{I_R}_{mB}$ is the appropriate Clebsch-Gordan coefficient for the coupling of the isospins of the baryon and the meson to the isospin I_R of the resonance.

We note that we use — in contrast to Ref. [21] — relativistic propagators in Eqs. (1) and (4) and momentum-dependent widths in the spectral functions of the outgoing particles. However, this has only a very small effect on the resonance production cross sections and does not require a readjustment of the resonance parameters.

The mesonic resonances are treated analogously to the baryonic ones; i.e., their two-body decay widths are calculated according to Eq. (2). The parameters used are given in Table I. The three-pion decay width of the ω meson is assumed to be constant since it is very small.

B. Collision term

1. Baryon-baryon collisions

For invariant energies $\sqrt{s}<2.6$ GeV we describe baryon-baryon collisions as in Ref. [11] with the same matrix elements. Our modified treatment of the resonance properties preserves the very good agreement with the experimental data on one- and two-pion production in nucleon-nucleon collisions shown in Ref. [11]. For higher energies we use the string fragmentation model FRITIOF [13] with the same parameters as in Ref. [23]. This approach is similar to the ones in the hadronic transport models described in Refs. [24,25].

2. Meson-baryon collisions

For meson-baryon collisions we use the string fragmentation model for $\sqrt{s}>2.2$ GeV. For lower energies the most important contributions come from intermediate nucleon resonances which are described according to Eq. (1).

In the case of π^-p scattering the incoherent sum of all resonance contributions gives a very good agreement with experimental data for pion momenta $p_\pi\leqslant 1.1$ GeV, corresponding to invariant energies $\sqrt{s}\leqslant 1.73$ GeV. In Fig. 1 we show the total π^-p cross section. For higher energies ($1.73\ {\rm GeV}<\sqrt{s}<2.2$ GeV) we additionally include a background $\pi N\to\pi\pi N$ cross section in order to reproduce the total cross section for which we use a parametrization from the PDG [26] (shown as solid line in Fig. 1). In Fig. 2 we show that the resonance contributions give a very good description of experimental data on elastic scattering, charge exchange, and two-pion and eta production cross sections.

For π^+p scattering one gets, also for lower energies, good agreement with experimental data only if one takes into

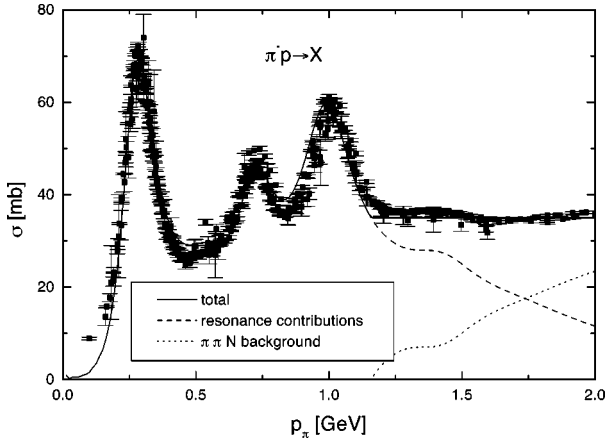

FIG. 1. The total $\pi^- p$ cross section compared to the experimental data from [49].

account all resonances from Ref. [21], including the one-star ones, as can be seen from Figs. 3 and 4. Since we do not explicitly propagate the one-star resonances we put their contributions into background cross sections for $\pi N \to \pi N$ and $\pi N \to \pi\pi N$. For higher energies we, again, include a two-pion production background term that is fitted to the total cross section from Ref. [26].

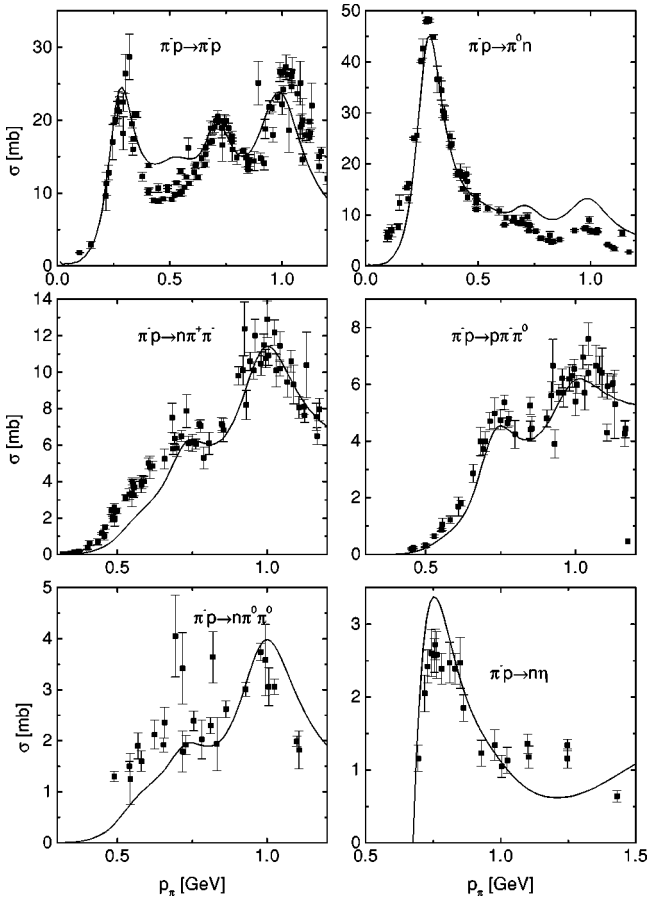

FIG. 2. $\pi^- p$ cross sections for elastic scattering, charge exchange, and two-pion and eta production. The experimental data are taken from [49].

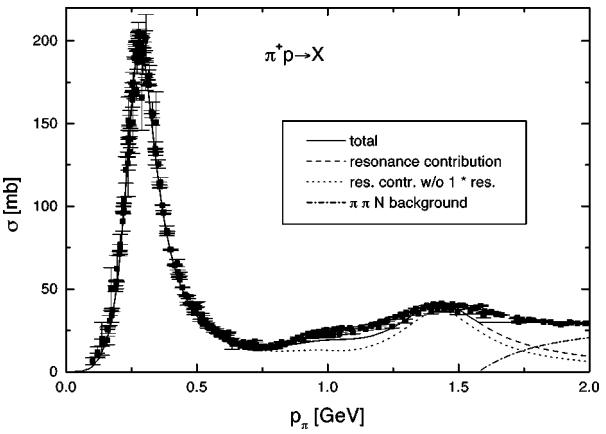

FIG. 3. The total $\pi^+ p$ cross section compared to the experimental data from [49].

For $\pi^0 p$ scattering we have, from isospin symmetry,

$$\sigma_{\pi^0 p} = \frac{1}{2}(\sigma_{\pi^+ p} + \sigma_{\pi^- p})$$

for the total cross section. The cross sections for pion-neutron scattering also follow from isospin symmetry.

In Fig. 5 we compare the resonance contributions to $\pi^- p \to n\rho^0$ to the experimental data from Ref. [27]. While for invariant energies $\sqrt{s}$ above 1.8 GeV the experimental data are reasonably well described by the resonances, there is a strong disagreement at lower energies, in particular in the region of the $D_{13}(1520)$ resonance. The ρ mesons produced at these energies have invariant masses essentially below the pole mass m_ρ^0. In Ref. [27] the ρ-meson cross section has been obtained by a fit to invariant mass spectra of the outgoing pions in $\pi^- p \to n\pi^+\pi^-$. For low $\sqrt{s}$ the shapes of the ρ meson and the ''background'' contributions become very similar and a determination of the ρ-meson cross section gets very difficult.

In Ref. [21] the couplings of the baryonic resonances to the $N\rho$ channel have been determined by using amplitudes

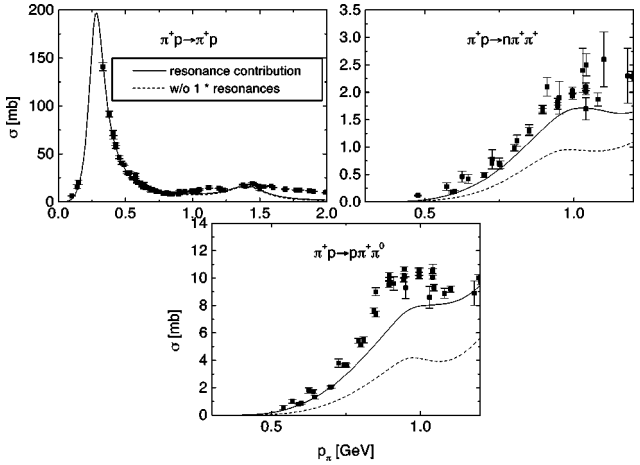

FIG. 4. $\pi^+ p$ cross sections for elastic scattering and two-pion production. The experimental data are taken from [49].

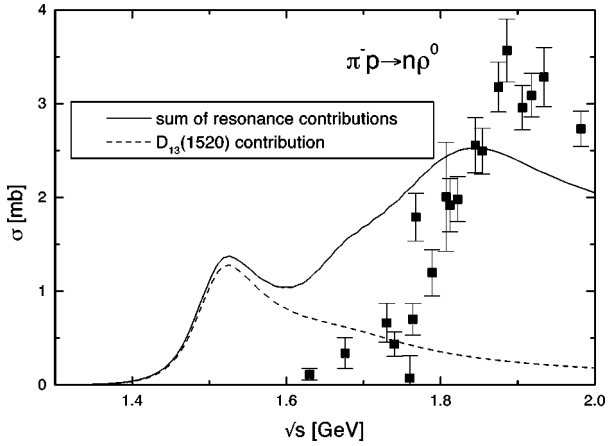

FIG. 5. Cross section for $\pi^- p \to n\rho^0$. The experimental data are taken from Ref. [27].

for $\pi N \to N\rho$ that were obtained by a partial wave analysis of all available $\pi N \to N\pi\pi$ data in Ref. [28]. We also note that the large coupling of the $D_{13}(1520)$ resonance to the $N\rho$ channel found in Ref. [21] is in line with other similar analyses [29]. Therefore we consider the experimental data in Ref. [27] to be wrong for low $\sqrt{s}$.

In addition to the resonance contributions we include the following processes:

$$\pi N \leftrightarrow \omega N,$$

$$\pi N \to \omega \pi N,$$

$$\omega N \to \pi\pi N,$$

$$\omega N \to \omega N,$$

$$\pi N \leftrightarrow \phi N,$$

$$\pi N \to \phi \pi N,$$

$$\phi N \to \pi\pi N,$$

$$\phi N \to \phi N,$$

where we adopt the cross sections from Ref. [30]. For cross sections involving an ω meson we, of course, subtract our resonance contributions from these cross sections.

C. Treatment of broad resonances

In our model broad resonances, like the baryon resonances or the ρ meson, are not just produced and propagated with their pole mass but according to their spectral function. The transport equation for a system of N particle species reads

$$\left(\frac{\partial}{\partial t}+\frac{\partial H_i}{\partial \vec{p}}\frac{\partial}{\partial \vec{r}}-\frac{\partial H_i}{\partial \vec{r}}\frac{\partial}{\partial \vec{p}}\right)F_i = G_i\mathcal{A}_i - L_i F_i \quad (i=1,\ldots,N), \tag{7}$$

where $F_i(\vec{r},\vec{p},\mu,t)$ denotes the one-particle spectral phase space density of particle species i with $\vec{r}$ and $\vec{p}$ being the spatial and momentum coordinates of the particle. μ is the invariant mass of the particle and $H_i(\vec{r},\vec{p},\mu,F_1,\ldots,F_N)$ stands for the single-particle mean field Hamilton function which, in our numerical realization [11], is given as

$$H_i = \sqrt{(\mu+S_i)^2+\vec{p}^2}, \tag{8}$$

where $S_i(\vec{r},\vec{p},\mu,F_1,\ldots,F_N)$ is a scalar potential. We note that we neglect a vector potential and S_i is an effective scalar potential that is — for the nucleons — obtained from a nonrelativistic potential (for details see Ref. [11]). The terms $G_i(\vec{r},\vec{p},\mu,F_1,\ldots,F_N)$ and $L_i(\vec{r},\vec{p},\mu,F_1,\ldots,F_N)$ stand for a gain and a loss term, respectively, and $\mathcal{A}_i(\vec{r},\vec{p},\mu,F_1,\ldots,F_N)$ is the spectral function of particle i. The distribution function f_i is defined by

$$f_i(\vec{r},\vec{p},\mu,t) = \frac{F_i(\vec{r},\vec{p},\mu,t)}{\mathcal{A}_i(\vec{r},\vec{p},\mu,t)}; \tag{9}$$

for stable particles it reduces to the usual phase space density.

In order to be more specific about G_i and L_i let us consider, as an example, a system of nucleons, rho mesons, pions, and a single baryonic resonance species R that are coupled only via $R \leftrightarrow N\rho$ and $\rho \to \pi\pi$. Then the gain term G_ρ is

$$G_\rho = \frac{1}{\mathcal{A}_\rho}\int \frac{d^3p_R}{(2\pi)^3} d\mu_R F_R(\vec{r},\vec{p}_R,\mu_R,t)\frac{d\Gamma_{R\to N\rho}}{d^3p_\rho d\mu_\rho} \times[1-f_n(\vec{r},\vec{p}_n,t)], \tag{10}$$

where the factor $(1-f_n)$ accounts for the Pauli principle of the outgoing nucleon and $\vec{p}_n = \vec{p}_R - \vec{p}_\rho$ due to momentum conservation. For simplicity, we have neglected a possible finite width of the nucleons as well as a Bose enhancement factor $(1+f_\rho)$ for the ρ meson. In the differential decay width $d\Gamma_{R\to N\rho}$ the spectral function of the ρ meson $\mathcal{A}_\rho$ enters simply as a multiplicative factor [Eqs. (2) and (3)]. Therefore, here G_ρ does not depend on $\mathcal{A}_\rho$ since we neglect any process where more than one ρ-meson is produced, like, e.g., $R \to \rho\rho N$.

The loss term L_ρ reads

$$L_\rho = \Gamma_{\rho\to\pi\pi} + \int \frac{d^3p_n}{(2\pi)^3} f_n(\vec{r},\vec{p}_n,t) v_{n\rho}\sigma_{\rho n\to R}, \tag{11}$$

with $v_{n\rho}$ being the relative velocity of the nucleon and the ρ meson and $\sigma_{\rho n\to R}$ their cross section for the production of resonance R [Eq. (1)]. $\Gamma_{\rho\to\pi\pi}$ denotes the two-pion decay width of the ρ meson in the calculational frame.

The total in-medium width $\Gamma_{\mathrm{tot},\rho}$ appearing in the spectral function from Eq. (4) is directly related to the loss rate L_ρ:

$$\Gamma_{\mathrm{tot},\rho} = \gamma L_\rho, \tag{12}$$

where γ is a Lorentz factor which appears since $\Gamma_{\mathrm{tot},\rho}$ is the decay rate in the rest frame of the ρ meson.

The loss and gain terms for the resonance R can be written down in an analogous way. One immediately sees that the transport equations of the ρ meson and the resonance R are coupled in a highly nonlinear way. Especially the in-medium widths, which are functions of space-time and four-momentum, of both particles depend on each other through integral equations [Eqs. (1), (2), (3), (4), and (11)].

The above-described equations can easily be extended to a transport model with more particle species and a realistic collision term. We also note that it is straightforward to formulate the theory consistently for the real and imaginary parts of the self-energies of the particles. However, in our model we treat the real and imaginary parts of the self-energies completely independently. This violates analyticity, but in the present stage it would already require a considerable effort to treat the imaginary parts of all particles in a realistic transport model in a completely self-consistent way.

In Ref. [31] it has recently been stressed that, because of unitarity, it is important to respect Eq. (12) in transport calculations. This means that in the population of a resonance the same width has to be used in the spectral function that enters the dynamical calculation via the collision term. In Refs. [12,32] we have already taken into account the in-medium widths of the baryonic resonances $\Delta(1232)$, $N(1520)$, $N(1535)$, and $N(1680)$ in a consistent way for population and propagation. Since during a photoproduction reaction the nucleus remains, in the time interval relevant for meson production, close to its ground state, the calculational effort is in this case manageable. As we describe the nuclear ground state in a local Thomas-Fermi approximation we can use nuclear matter values for the in-medium widths that depend only on the invariant mass μ, the absolute value of the three-momentum $|\vec{p}|$, and the density ρ:

$$\Gamma(\vec{r},t,\vec{p},\mu)\rightarrow\Gamma(\rho(\vec{r},t),|\vec{p}|,\mu).$$

In the present paper we only take into account the in-medium widths of the ρ and ω mesons. In particular, we neglect any medium-modifications of the $N\rho$ widths of the baryonic resonances that would, in a self-consistent calculation of the self-energies, directly follow from a modification of the spectral function of the ρ meson. As was shown in Ref. [33] such effects might give large modifications of the baryon widths and also influence the spectral function of the ρ meson. However, an inclusion of such effects would enhance the numerical effort dramatically, especially if one takes also the modifications of the real parts of the self-energies into account. Moreover, we do not expect such effects to be relevant for photon energies above 1 GeV because here the nucleon resonances that lie below $M_N+m_\rho^0$ and might thus get strongly modified, like the $D_{13}(1520)$, play only a minor role. Observable effects of different medium modifications of the D_{13} will be reported elsewhere.

The transport equations (7) do not yet give the correct asymptotic spectral phase space densities for particles that are stable in the vacuum. This can be seen by noting that a collision broadened particle does not automatically lose its collisional width when being propagated out of the nuclear environment. The same problem appears for resonances whose imaginary part of the self-energy is nonzero in-medium in kinematical regimes where it is zero in vacuum.

The reason for this deficiency is directly related to the semiclassical approximations on which the transport equation (7) is based, in particular the neglect of coherence effects. However, since a realistic quantum transport theory is numerically not yet realizable, we will nevertheless work with Eq. (7) as it is certainly a step beyond the usual on-shell approximation. Moreover, if the time evolution of the system is such that the rate of particle production and absorption is much larger than the change of the width with time, the problem with surviving off-shell contributions will be negligible. Under the assumption that the gain term in the collision term is in magnitude comparable to the loss term we can formulate this in the following way:

$$\Gamma dt \gg \frac{d\Gamma}{\Gamma}. \tag{13}$$

In case of a particle moving in a static nuclear medium with density profile $\rho(\vec{r})$ we can rewrite this condition:

$$\frac{\vec{\nabla}\rho\cdot\vec{e}_p}{\rho} \ll \frac{1}{\lambda}, \tag{14}$$

where $\vec{e}_p$ is a unit vector along the momentum direction of the particle and λ denotes its mean free path. In Sec. IV A we will discuss the validity of this condition for our calculations and present possible remedies to the problem.

D. Parametrization of the elementary γN cross sections

For invariant energies $\sqrt{s}<2.1$ GeV, corresponding to $E_\gamma<1.88$ GeV on a free nucleon at rest, we describe one-pion, two-pion, and eta production as in Ref. [12]. For the two-pion production cross sections on the neutron we meanwhile use the experimental data from Refs. [34,35] instead of the recipe described in Ref. [12]. For larger energies we use, like for the hadronic interactions, the string fragmentation model FRITIOF where we initialize a zero-mass ρ^0 meson for the photon following a vector-meson dominance (VMD) picture. For the total cross section we use a parametrization from Ref. [26]. The Lund model is then used to determine the probabilities for the different final states. In Fig. 6 we show that this gives a very good description of charged particle multiplicities in photon-proton collisions; the agreement seen there is better than could be expected from a model that had been developed for applications at high energies. However, we do not expect the Lund model to give correct predictions for all specific channels, especially with respect to isospin. The role of the Lund model for our calculations is to supply us with an overall description of the elementary reaction dynamics in order to allow us to take into account multistep processes where, for example, a primary produced pion produces a vector meson on a second nucleon.

The vector-meson (ρ,ω,ϕ) production in $\gamma N\rightarrow VN$ collisions is fitted to experimental data [36,37] and treated inde-

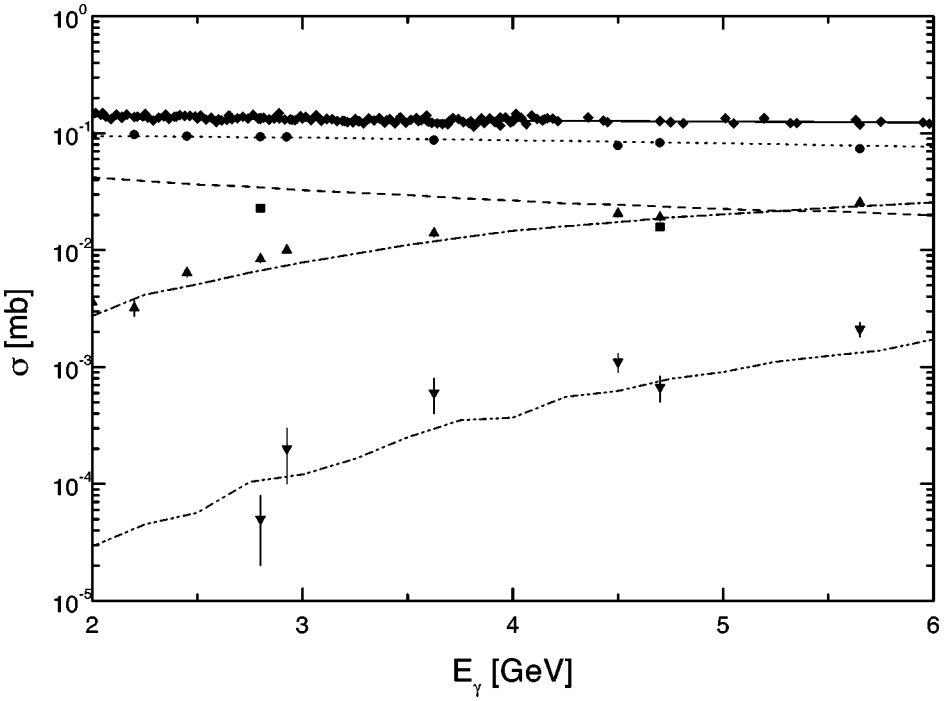

FIG. 6. Charged particle multiplicity cross sections in γp reactions: $\gamma p \rightarrow 1$ charged particle [dashed line (calculation as described in the text), squares (experimental data from Ref. [49])], three charged particles (dotted line, circles), five charged particles (dot-dashed line, up triangles), and seven charged particles (dot-dot-dashed line, down triangles). Also shown is the total cross section (solid line, rhombs).

pendent of the Lund model also for high energies. The cross section is given as

$$\sigma_{\gamma N \rightarrow NV} = \frac{1}{p_i s} \int d\mu |\mathcal{M}_V|^2 p_f \mathcal{A}_V(\mu), \tag{15}$$

where $\sqrt{s}$ is the total energy of the γN system, p_i, p_f are the momenta of the initial and final particles in the center-of-mass system, and $\mathcal{A}_V$ is the spectral function of vector meson V [Eq. (4)]. The matrix elements $\mathcal{M}_V$ are parametrized in the following way:

$$|\mathcal{M}_\rho|^2 = 0.16 \ \text{mb GeV}^2,$$

$$|\mathcal{M}_\omega|^2 = \frac{0.08 p_f^2}{2(\sqrt{s} - 1.73\text{GeV})^2 + p_f^2} \ \text{mb GeV}^2,$$

$$|\mathcal{M}_\phi|^2 = 0.004 \ \text{mb GeV}^2. \tag{16}$$

In Fig. 7 we show the resulting cross sections (dash-dotted curves) for $\gamma p \rightarrow p \rho^0$ (upper part), $\gamma p \rightarrow p \omega$ (middle part), and $\gamma p \rightarrow p \phi$ (lower part) in comparison with the experimental data. For the angular distribution of the produced vector mesons we use

$$\frac{d\sigma}{dt} \propto \exp(Bt), \tag{17}$$

where t denotes the square of the four-momentum transfer of the photon to the vector meson. In Ref. [36] the parameter B was, depending on photon energy, fitted to ρ^0 production. Here, we adopt these values and also use them for ω and ϕ production.

In our calculations there is an additional contribution to $\gamma N \rightarrow N \rho^0$ coming from the decays of the $N(1520)$ and $N(1680)$ resonances which is shown in Fig. 7 by the dashed line. These decays predominantly contribute to low mass ρ mesons below the experimentally seen ρ production threshold.

Besides the exclusive process $\gamma N \rightarrow VN$ we also have, for the photon energies considered here, to take into account additional channels for the photoproduction of vector mesons. For energies above 2.1 GeV we calculate these cross sections using the Lund model. Below 2.1 GeV we absorb everything into the channel $\gamma N \rightarrow V \pi N$ for which we use the following cross section:

$$\sigma_{\gamma N \rightarrow V \pi N} = \frac{16(2\pi)^7}{p_i \sqrt{s}} \int d\mu d\Phi_3 |\mathcal{M}_{V\pi}|^2 \mathcal{A}_V(\mu), \tag{18}$$

where $d\Phi_3$ denotes the three-body phase space element as, for example, given by Eq. (35.11) in Ref. [20]. The matrix elements are adjusted to give a continuous transition to the string fragmentation model at $\sqrt{s} = 2.1$ GeV. We use

$$|\mathcal{M}_{\rho^0 \pi}|^2 = |\mathcal{M}_{\omega \pi}|^2 = 0.5 \ \text{mb}.$$

The calculated inclusive rho and omega production cross sections (after subtraction of the exclusive part) are shown as dotted lines in Fig. 7. The total inclusive vector-meson production cross sections are indicated as solid lines.

For photon energies above 1 GeV we take into account nuclear shadowing of the incoming photon by adopting the model of Ref. [38]. Since this has, for the photon energies considered here, only a small impact on the final results, our specific transport theoretical realization will be described elsewhere [39].

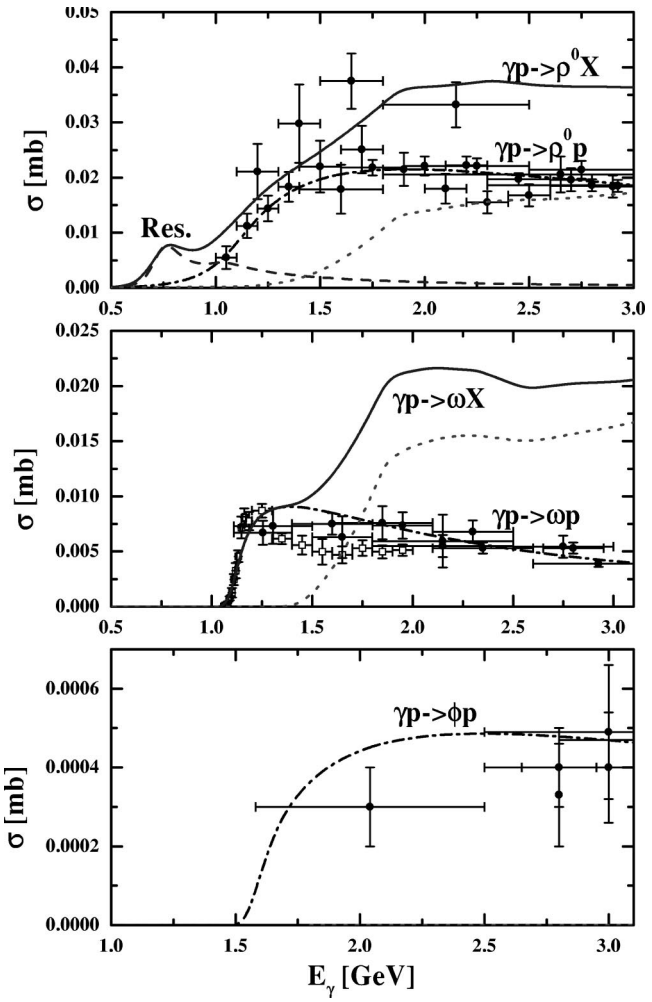

FIG. 7. The ρ (upper part), ω (middle part) and ϕ (lower part) meson production cross section for γp reactions. The experimental data corresponding to the exclusive reactions $\gamma p \rightarrow Vp$ ($V=\rho,\omega,\phi$) are taken from Ref. [36] (solid circles) and from Ref. [37] (open squares). The dash-dotted lines are our parametrization of the exclusive data; the dashed line (upper part) is the resonance contribution. The dotted lines indicate the calculated inclusive vector-meson production cross section (see text); the solid lines correspond to the total vector-meson production cross section.

E. Dilepton production

In our analysis we calculate dilepton production by taking into account the contributions from the Dalitz decays $\Delta \rightarrow Ne^+e^-$, $\eta \rightarrow \gamma e^+e^-$, $\omega \rightarrow \pi^0 e^+e^-$, and $\pi^0 \rightarrow \gamma e^+e^-$ and the direct dilepton decays of the vector mesons ρ,ω,ϕ.

The Dalitz decays of the π^0 and the η are parametrized according to Ref. [41]. For the Dalitz decay of the ω we use the parametrization from Ref. [40]. The Δ Dalitz decay is described in line with Ref. [42] where we, however, use $g=5.44$ for the coupling constant in order to reproduce the photonic decay width $\Gamma_0(0)=0.72$ MeV.

The dilepton decay of the vector mesons is calculated assuming strict vector-meson dominance [43] as in Ref. [7]:

$$\Gamma_{V\rightarrow e^+e^-}(M)=C_V\frac{m_V^4}{M^3}, \tag{19}$$

where $C_\rho=8.814\times10^{-6}$, $C_\omega=0.767\times10^{-6}$, and $C_\phi=1.344\times10^{-6}$, respectively [20]. Within an extended vector-meson dominance picture [44] one has a dilepton decay amplitude that consists of two terms, one describing the coupling of the virtual photon to the hadron with a strength proportional to M^2 and another with strength proportional to M^0. However, since we neglect a direct coupling of the virtual photon, the use of strict vector-meson dominance is more appropriate. We also note that this dilepton decay width together with our parameters for the ρ meson gives a very good description of the experimental data for $e^+e^- \rightarrow \pi^+\pi^-$.

In our transport model the dilepton yield is obtained from the phase space distributions of the respective sources by a time integration. For the vector mesons the mass differential dilepton production is given as

$$\frac{dN_{V\rightarrow e^+e^-}}{d\mu}=\int_0^\infty dt\, d^3r\frac{d^3p}{(2\pi)^3}F_V(\vec{r},t,\vec{p},\mu)\,\frac{\Gamma_{V\rightarrow e^+e^-}}{\gamma}, \tag{20}$$

where γ is a Lorentz factor which appears since $\Gamma_{V\rightarrow e^+e^-}$ is the width in the rest frame of the vector meson. The Dalitz decay contributions contain an additional mass integration. For the Δ resonance we have, for example,

$$\frac{dN_{\Delta\rightarrow Ne^+e^-}}{d\mu}=\int_0^\infty dt\, d^3r\frac{d^3p}{(2\pi)^3}d\mu_2 F_\Delta(\vec{r},t,\vec{p},\mu_2)\frac{1}{\gamma} \times\frac{d\Gamma_{\Delta\rightarrow Ne^+e^-}}{d\mu}. \tag{21}$$

III. DILEPTON PRODUCTION IN γA REACTIONS

A. Hadronic contribution

In Figs. 8–10 we present the calculated dilepton spectra $d\sigma/dM$ for γC, γCa, and γPb reactions at photon energies $E_\gamma=0.8$, 1.5, and 2.2 GeV. A mass resolution of 10 MeV is included through a convolution of our calculated spectrum with a Gaussian. Here neither collisional broadening nor a mass shift of the vector mesons were taken into account.

The thin lines indicate the individual contributions from the different production channels; i.e., starting from low M: Dalitz decay $\pi^0\rightarrow\gamma e^+e^-$ (short-dotted line), $\eta\rightarrow\gamma e^+e^-$ (dotted line), $\Delta\rightarrow Ne^+e^-$ (dot-dashed line), and $\omega\rightarrow\pi^0e^+e^-$ (dot-dot-dashed line); for $M\approx0.8$ GeV: $\rho^0\rightarrow e^+e^-$ (dashed line), $\omega\rightarrow e^+e^-$ (dot-dot-dashed line), and $\phi\rightarrow e^+e^-$ (dashed line). The solid lines represent the sum of all sources. The dominant processes in the low mass region up to $M\simeq500$ MeV are the η, ω, and Δ Dalitz decays. Above $M\sim0.6$ GeV the spectrum is dominated by the vector-meson decays with a low background from other hadronic sources.

In our calculations we only take into account ρ mesons with masses above $2m_\pi$ which is the threshold of the strong decay since in the calculation of the spectral function [Eq. (4)] we neglect contributions from electroweak decays. Therefore we get a discontinuity of our spectra in Figs. 8–10

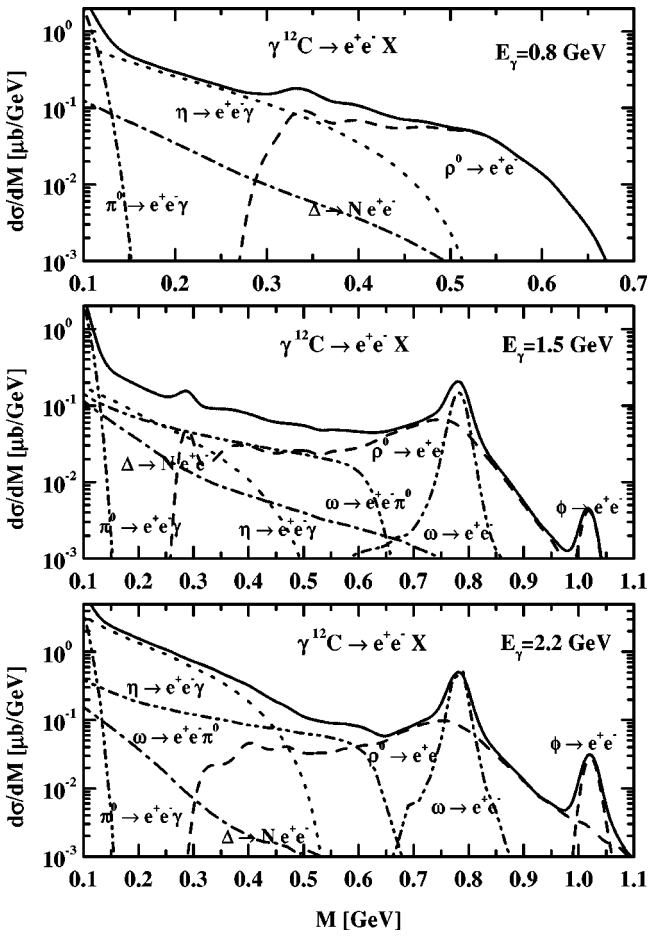

FIG. 8. The dilepton invariant mass spectra $d\sigma/dM$ for γC at the energy of $E_\gamma = 0.8$ GeV (upper part), 1.5 GeV (middle part), and 2.2 GeV (lower part) calculated with bare meson masses including a mass resolution of 10 MeV. The thin lines indicate the individual contributions from the different production channels; i.e., starting from low M: Dalitz decay $\pi^0 \rightarrow \gamma e^+ e^-$ (short-dotted line), $\eta \rightarrow \gamma e^+ e^-$ (dotted line), $\Delta \rightarrow N e^+ e^-$ (dot-dashed line), and $\omega \rightarrow \pi^0 e^+ e^-$ (dot-dot-dashed line); for $M \approx 0.8$ GeV: $\omega \rightarrow e^+ e^-$ (dot-dot-dashed line) and $\rho^0 \rightarrow e^+ e^-$ (dashed line). The solid line represents the sum of all sources.

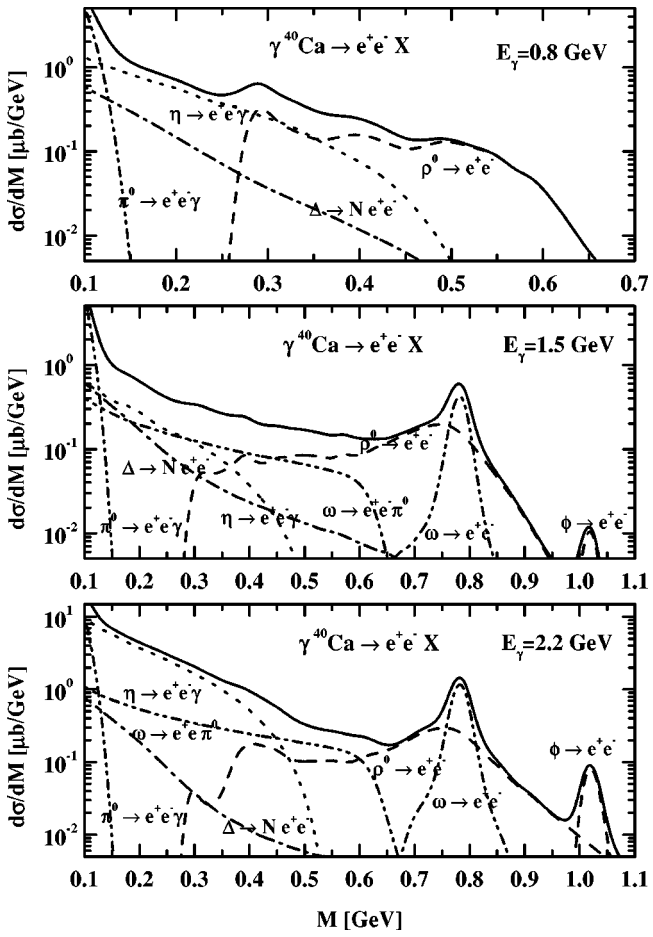

FIG. 9. The dilepton invariant mass spectra $d\sigma/dM$ for γCa at the energy of $E_\gamma = 0.8$ GeV (upper part), 1.5 GeV (middle part), and 2.2 GeV (lower part) calculated with bare meson masses including a mass resolution of 10 MeV. The assignment is the same as in Fig. 8.

at the two-pion mass that is, however, because of the other sources and the mass resolution hardly visible.

B. Bethe-Heitler contribution

Besides the ''hadronic'' contributions as discussed above we also have to take into account dilepton production via the so-called Bethe-Heitler (BH) process for which the Feynman diagrams are depicted in Fig. 11 that contribute to lowest order in the electromagnetic coupling constant α.

On a single nucleon, with the electromagnetic form factors known from electron scattering, the BH process is completely determined by quantum electrodynamics (QED) and can easily be calculated. For a detailed description of the involved matrix elements we refer to Ref. [45] from which we also adopted the parametrizations of the electromagnetic form factors $W_1(Q^2,\nu)$ and $W_2(Q^2,\nu)$ of the nucleon.

For our calculations we take only the incoherent sum over BH contributions on single nucleons into account and neglect contributions where the intermediate photon couples to the charge of the whole nucleus. While the latter will, because of the Z^2 dependence, dominate all integrated cross sections, it can experimentally easily be suppressed by appropriate missing mass cuts.

In Fig. 12 we compare the BH contributions for γPb at 1.5 (upper part) and 2.2 GeV (lower part) with the ''hadronic'' contributions that we have already shown in Fig. 10. One sees that the sum of the elementary cross sections on the proton and the neutron (dashed lines) is much larger than the ''hadronic'' contributions (solid lines) for dilepton masses below 0.6 GeV. In the region of the ρ and ω mesons the BH contribution is about a factor of 4 smaller but still non-negligible. With the inclusion of Fermi motion and Pauli blocking (dotted lines) the BH contribution is reduced significantly for low invariant masses but hardly affected for masses larger than 700 MeV.

In order to suppress the BH contribution we implemented the cuts $(k \cdot p),(k \cdot p_+) > 0.01$ GeV^2, where k is the four-momentum of the incoming photon, and p, p_+ are the four-

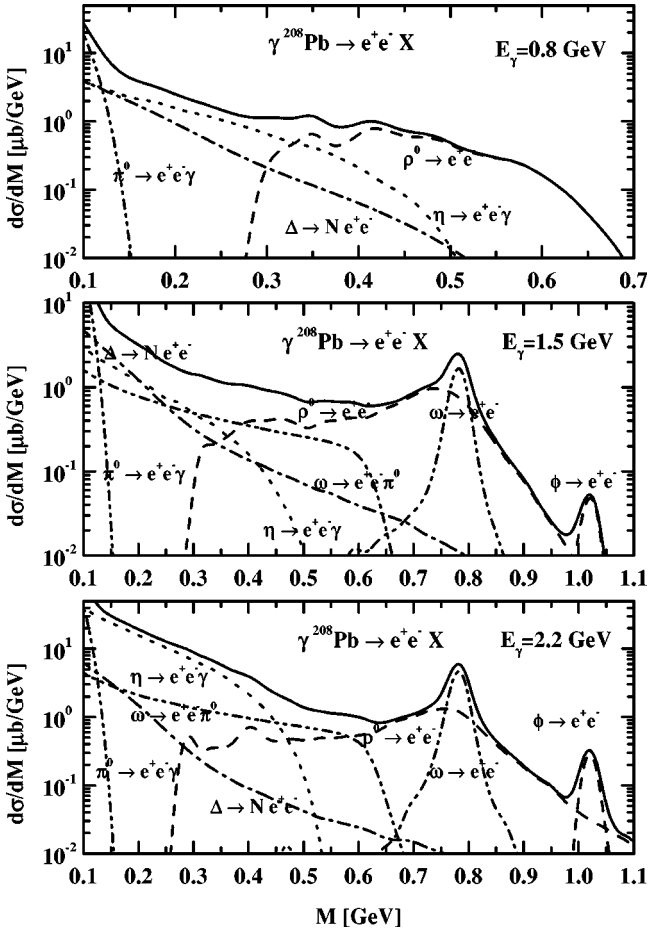

FIG. 10. The dilepton invariant mass spectra $d\sigma/dM$ for γPb at the energy of $E_\gamma = 0.8$ GeV (upper part), 1.5 GeV (middle part), and 2.2 GeV (lower part) calculated with bare meson masses including a mass resolution of 10 MeV. The assignment is the same as in Fig. 8.

momenta of electron and positron, respectively. These cuts, which reflect the polelike behavior of the intermediate electron propagator, suppress the BH contribution by a factor of 10 — dot-dashed lines in Fig. 12 — and practically do not have any influence on the ''hadronic'' contributions.

In our calculations we do not take into account interference terms between the BH and the ''hadronic'' contributions. In inclusive reactions in which one sums both over the e^+e^- pair and that pair in which e^+ and e^- are exchanged the total contribution from the interference term vanishes.

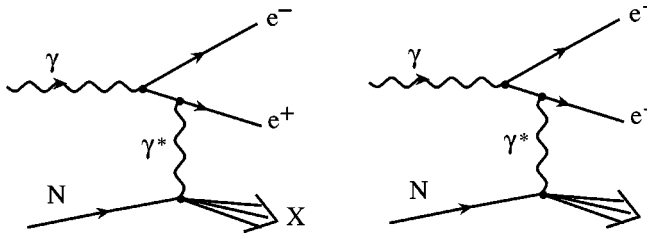

FIG. 11. Feynman diagram for $\gamma N \to e^+e^-X$ for the Bethe-Heitler process.

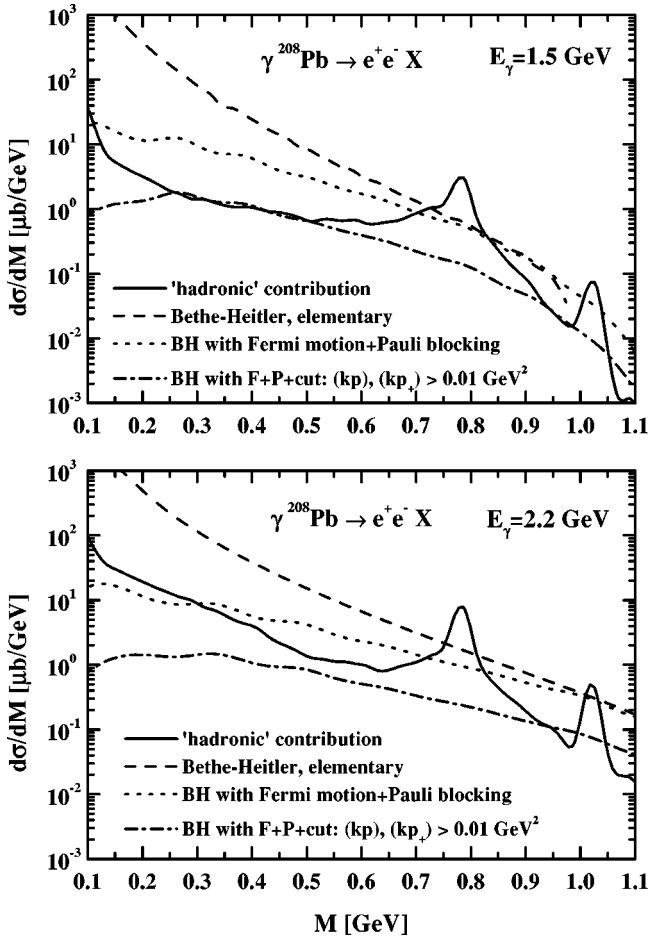

FIG. 12. The dilepton invariant mass spectra $d\sigma/dM$ for γPb at the energy of $E_\gamma = 1.5$ GeV (upper part) and 2.2 GeV (lower part). The solid lines indicate the ''hadronic'' spectra as in Fig. 10. The dashed lines are the Bethe-Heitler contribution calculated as a sum of incoherent contributions from γ+nucleons. The dotted lines show the BH yield with taking into account nucleon Fermi motion and Pauli blocking. The dot-dashed lines are the BH terms with the cuts $(kp),(kp_+) > 0.01$ GeV.

Therefore, the BH contribution can be separated. We thus discuss in the following only the hadronic component.

IV. IN-MEDIUM EFFECTS IN DILEPTON PRODUCTION

A. Collisional broadening

The in-medium widths of the ρ and ω mesons are calculated as sketched in Sec. II C. In the rest frame of the meson the total in-medium width is given as

$$\Gamma^V_{\rm tot}(\mu,|\vec{p}|,\rho) = \Gamma^V_{\rm vac}(\mu) + \Gamma^V_{\rm coll}(\mu,|\vec{p}|,\rho), \qquad (22)$$

where the collisional width $\Gamma^V_{\rm coll}$ reads

$$\Gamma^V_{\rm coll}(\mu,|\vec{p}|,\rho) = \gamma\rho\langle v_{VN}\sigma^{\rm tot}_{VN}\rangle, \qquad (23)$$

and $\Gamma^V_{\rm vac}$ is the vacuum decay width. In Eq. (23) the brackets stand for an average over the Fermi sea of the nucleons, v_{VN} is the relative velocity between vector meson and nucleon,

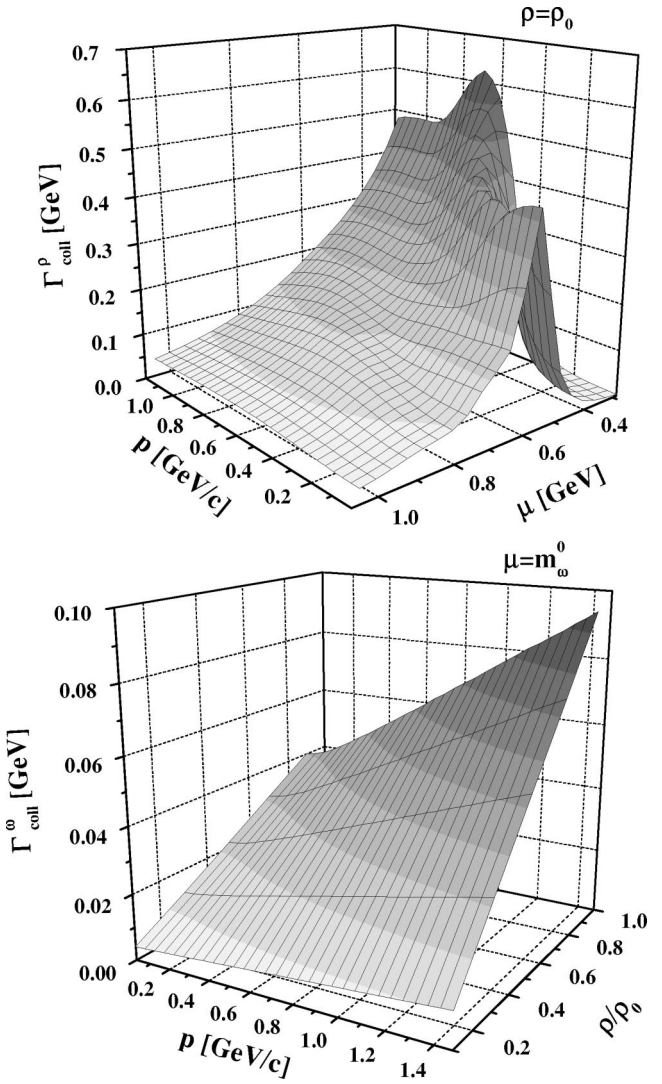

FIG. 13. The upper part shows the collisional width of the ρ meson as a function of momentum and mass at normal nuclear density $\rho=\rho_0$. The lower part is the momentum and density dependence of the ω collisional width calculated at $\mu=m_\omega^0$.

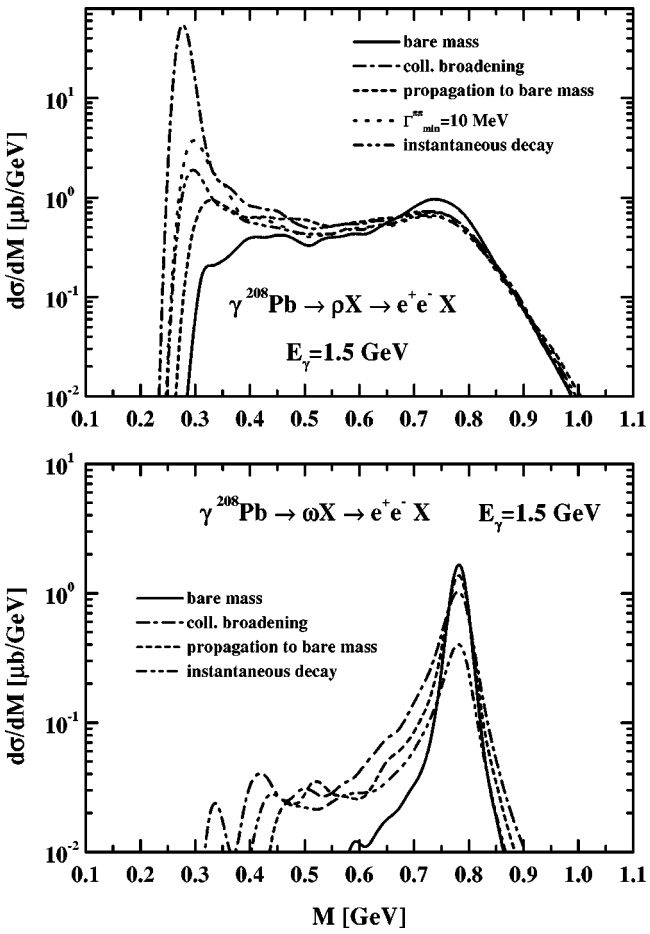

FIG. 14. The dilepton yield from ρ (upper part) and ω (lower part) meson decays for γPb at 1.5 GeV calculated within different prescriptions: the solid lines are the results with bare mass, the dot-dashed lines indicate the calculation with collisional broadening, the dot-dot-dashed lines correspond to the instantaneous decay, the dotted line (upper part) is the result with $\Gamma_{\min}^{\pi\pi}=10$ MeV, and the short dashed lines indicate the yield calculated with the ''propagation to bare mass'' prescription.

and $\sigma_{VN}^{\rm tot}$ is their total cross section. ρ is the nuclear density and γ the Lorentz factor for the boost to the rest frame of the vector meson.

The upper part of Fig. 13 shows the collisional width of the ρ meson as a function of momentum and mass at nuclear matter density $\rho=\rho_0$. The structure at low μ comes from the resonance contributions, especially from the $D_{13}(1520)$. Note that the width becomes very large (up to about 600 MeV), corresponding to a complete melting of the ρ meson. The lower part of Fig. 13 shows the momentum and density dependence of the ω collisional width calculated at the pole mass $\mu=m_\omega^0$. At nuclear matter density ρ_0 and a momentum of $p=1$ GeV we obtain a collisional width of about 80 MeV which is about a factor of 10 larger than the vacuum decay width.

1. Observable consequences

In Fig. 14 (upper part) we show the contribution of the ρ meson to the e^+e^- yield for γPb at 1.5 GeV. The solid line indicates the bare mass case (as in Fig. 10), i.e., without collisional broadening. The curve labeled ''coll. broadening'' (dash-dotted line) results if we take into account the collision broadening effect in the production of the ρ mesons. Here we calculate the ρ-meson production cross sections in photon-nucleon collisions [Eqs. (15) and (18)] with the in-medium spectral function. Since the in-medium spectral function depends on the momentum of the ρ meson with respect to the nuclear medium, an additional angular integration has to be performed. For the case of exclusive production $\gamma N\rightarrow N\rho$ we use the angular distribution from Eq. (17). For $\gamma N\rightarrow N\rho\pi$ we assume an isotropic three-body phase space distribution.

As discussed in Sec. II C we do not modify the $N\rho$ width of the baryonic resonances but the masses of the ρ mesons stemming from these decays are distributed according to the (phase space weighted) in-medium spectral function. We, again, neglect ρ mesons with masses below the two-pion threshold.

From Fig. 14 one sees that the inclusion of collisional broadening leads to a depletion of the ρ-meson peak by about 30% and a shift of strength to lower dilepton masses. One also observes a very large peak at $M=2m_\pi$ which is in fact a pole but here finite due to our numerical solution. The reason for this divergence is directly related to our discussion in Sec. II C of the asymptotic solutions of the semiclassical transport equation when including in-medium spectral functions. At the two-pion mass the vacuum spectral function of the ρ meson is zero while the in-medium spectral function has some finite value since the collision width from Eq. (23) does not vanish. When travelling to the vacuum the respective component of the spectral phase space density becomes infinitely long lived and leads to the divergence. If we included the electroweak decay width of the ρ meson into the collision term of the transport equation, the problem would not be solved. The pole would only be replaced by a numerically indistinguishable large peak.

In Fig. 14 (lower part) we show the contribution of the ω meson when including collisional broadening (dash-dotted line) in comparison to the calculation with the vacuum spectral function (solid line, as in Fig. 10). One observes a strong broadening of the ω peak which is partly covered up by the inclusion of a mass resolution of 10 MeV. However, such a strong broadening is not realistic because most of the ω mesons that contribute to the dilepton spectrum decay in the vacuum. This is also reflected by the violation of the condition (14) for the validity of our off-shell transport equation in this case.

2. Prescriptions to obtain correct asymptotic behavior

In the following we want to discuss a prescription that allow us to obtain a divergence-free ρ-meson and a reasonable ω-meson contribution. For that purpose we introduce a potential that shifts a particle to its vacuum spectral function when it propagates to the vacuum. Such a potential cannot be defined on the level of the transport equation (7). However, we can introduce such a potential on the level of our numerical realization. We recall that we solve the transport equation by a so-called test particle method; i.e., we make an ansatz for the spectral phase space density F:

$$F(\vec{r},t,\vec{p},\mu)\propto\sum_i \delta(\vec{r}-\vec{r}_i(t))\delta(\vec{p}-\vec{p}_i(t))\delta(\mu-\mu_i), \tag{24}$$

where $\vec{r}_i(t)$, $\vec{p}_i(t)$, and μ_i denote the spatial coordinate, the momentum, and the mass of the test particle i, respectively. Now, we can define for each test particle a density-dependent scalar potential s_i in the following way:

$$s_i(\rho_i(t))=(\mu_i^{\rm med}-\mu_i^{\rm vac})\frac{\rho_i(t)}{\rho_i^{\rm cr}}, \tag{25}$$

where $\mu_i^{\rm med}$ is the ''in-medium'' mass of the test particle chosen according to the mass differential production cross section. $\mu_i^{\rm vac}$ is the ''vacuum'' test particle mass which is chosen according to the production cross section with a vacuum spectral function. $\rho_i^{\rm cr}$ is the baryon density at the creation point, whereas $\rho_i(t)=\rho(\vec{r}_i(t))$ is the baryon density during the propagation. Setting the test particle mass μ_i to the ''vacuum'' mass $\mu_i^{\rm vac}$ the effective in-medium mass $\mu_i^\star$ is given as

$$\mu_i^\star(\rho_i(t))=\mu_i^{\rm vac}+s_i(\rho(t)). \tag{26}$$

Equation (26) gives the correct asymptotic behavior: the effective mass at the creation point is kept unchanged $[\mu_i^\star(\rho_i^{\rm cr})=\mu_i^{\rm med}]$; during the propagation the test particle mass changes linearly with density and outside the nucleus it becomes equal to the bare mass $\mu_i^\star(\rho_i=0)=\mu_i^{\rm vac}$. The potential s_i enters into the test particle propagation as a usual potential and therefore guarantees that this prescription does not violate energy conservation.[1]

The potential (25) can assume rather large values in the case of broad resonances even if the in-medium corrections are small. Its effect is, nevertheless, in this case negligible. As a check we have performed a calculation of the photoproduction of ρ mesons in which we distributed the masses $\mu_i^{\rm med}$ according to the vacuum spectral function. This gave practically the same result as the calculation without a potential since the lifetime of the ρ mesons is so short that only very few propagate through a relevant density gradient for which the potential becomes important.

In Fig. 14 we show the results of our calculations with the described prescription for the ρ and the ω mesons (curves labeled ''propagation to bare mass,'' dashed lines). For the ρ meson the divergence at the two-pion threshold is removed. For invariant masses above 500 MeV we get practically the same result as without the prescription because of the reason described in the preceding paragraph. The broadening of the ω peak is reduced because now only the ω mesons that decay inside the nucleus contribute to the broadening.

Another possibility to overcome the problems with the transport theoretical treatment of broad resonances is to avoid their explicit propagation. Therefore we have also performed simulations in which we calculated the cross sections for elementary dilepton production via vector mesons as instantaneous one-step processes. The results are shown in Fig. 14 by the curves labeled ''instantaneous decay'' (dot-dot-dashed lines). The ρ-meson contribution is almost identical to the one calculated with the prescription described above because of its very short lifetime. For the ω meson we get a reduction by about a factor of 3 since in the instantaneous decay scheme we neglect the possibility that an ω meson can escape from the nucleus and then contribute to dilepton production with a much larger branching ratio than inside the nucleus. As such dynamical effects are important to take into account we consider the description via an instantaneous process to be inadequate.

[1]After this paper was submitted two other papers dealing with the propagation of broad resonances appeared on the LANL preprint server [46,47].

The easiest way to cope with the divergence of the ρ-meson contribution is to use a minimum two-pion decay width. In Fig. 14 we show the result of a calculation where we set this minimum width to 10 MeV (dotted line). One sees that still a large peak remains. Moreover, this approach is in any case questionable.

For the reasons described above we consider the prescription ''propagation to bare mass'' as the only possibility to implement collision broadening effects in our calculations. However, we want to stress that this prescription is not fully satisfactory since it is only formulated on the level of our specific numerical solution of the transport equation and since it neglects any memory effects.

B. ''Dropping'' vector-meson mass

In order to explore the observable consequences of vector-meson mass shifts at finite nuclear density the in-medium vector-meson masses are modeled according to Brown-Rho scaling [3] or Hatsuda and Lee [4] by introducing a scalar potential $S_V(\vec{r})$:

$$S_V(\vec{r}) = -\alpha m_V^0 \frac{\rho(\vec{r})}{\rho_0}, \tag{27}$$

where $\rho(\vec{r})$ is the nuclear density, m_V^0 the pole mass of the vector meson, $\rho_0 = 0.168$ fm^{-3}, and $\alpha \simeq 0.18$ for the ρ and ω. The effective mass $\mu^\star$ is then given as

$$\mu^\star = \mu + S_V. \tag{28}$$

For the effective pole mass $\mu_0^\star$ we thus get

$$\mu_0^\star = \left(1 - \alpha \frac{\rho(\vec{r})}{\rho_0}\right) m_V^0.$$

In photon-nucleus reactions vector mesons are produced with large momenta relative to the nuclear medium. Within a resonance-hole model for the ρ-meson self-energy in the nuclear medium it has been shown in Ref. [48] that the real part of the in-medium ρ-meson self-energy increases with momentum and crosses zero for a momentum of about 1 GeV. In order to explore the implications of such a behavior we also use a momentum-dependent scalar potential $S_V^{\rm mom}$ for the vector mesons:

$$S_V^{\rm mom}(\vec{r},\vec{p}) = S_V(\vec{r})\left(1 - \frac{|\vec{p}|}{1\ \text{GeV}}\right). \tag{29}$$

In our calculations we take the vector-meson potentials into account for the calculation of the phase space factors in $\gamma N \to NV$ [Eq. (15)] and $\gamma N \to NV\pi$ [Eq. (18)]. We neglect these modifications for the vector-meson production in the string fragmentation model FRITIOF and also do not modify the $N\rho$ widths of the baryonic resonances.

C. Dileptons from γA reactions: In-medium effects

In Fig. 15 we show the contribution coming from the ω meson to e^+e^- production in γPb at a photon energy of 1.5

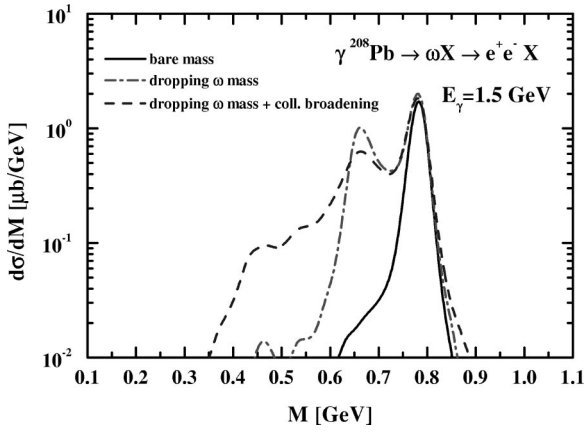

FIG. 15. The dilepton yield from ω mesons for γPb at 1.5 GeV. The solid line indicates the bare mass case, the dot-dashed line is the result with in-medium masses, and the dashed line shows the effect of collisional broadening together with the dropping mass.

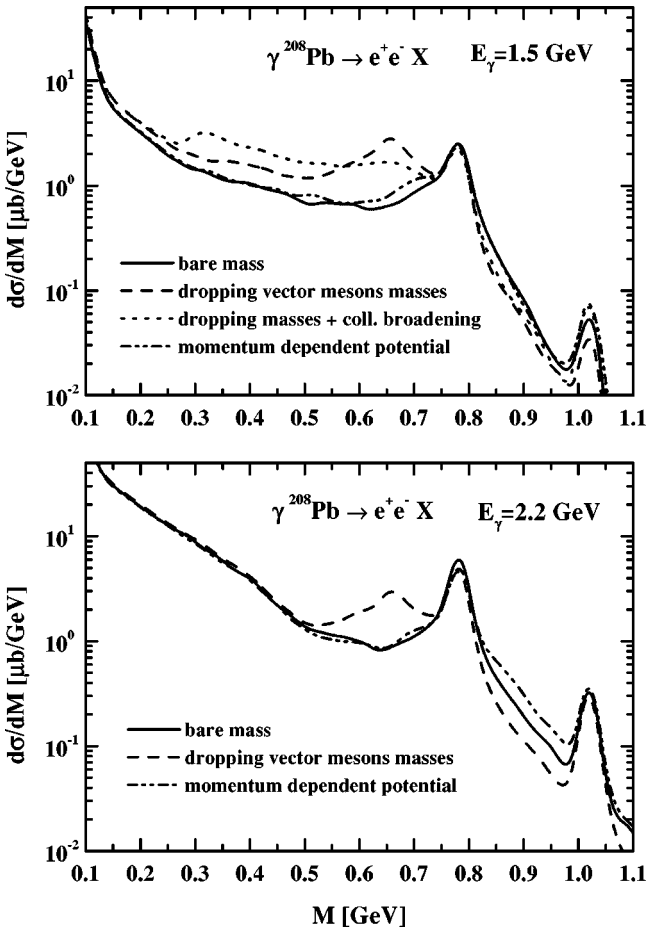

FIG. 16. The dilepton invariant mass spectra for γPb at 1.5 GeV (upper part) and 2.2 GeV (lower part). The solid lines indicate the bare mass case, the dashed lines are the result with the dropping mass scenario, the dotted line (upper part) shows the effect of collisional broadening together with the dropping mass, and the dot-dot-dashed lines indicate the result with the momentum-dependent potential from Eq. (29).

GeV. A dropping mass scenario according to Eq. (27) (dot-dashed line) gives a two-peak structure corresponding to ω mesons decaying inside and outside the nucleus, respectively. An additional inclusion of collisional broadening, as described in Sec. IV A, gives a substantial broadening of the dilepton yield from ω mesons that decay inside the nucleus. The height of the peak around the vacuum pole mass of the ω meson is hardly affected by the dropping mass scenario. On the one hand, the lowering of the mass reduces the vacuum peak because ω mesons decaying inside the nucleus contribute to lower masses. On the other hand, the total production of ω mesons is enhanced since the phase space factors entering the elementary photoproduction cross sections [Eqs. (15) and (18)] are increased for lower masses. In our calculation both effects nearly cancel each other for masses around the vacuum pole.

In Fig. 16 (upper part) we show the total e^+e^- yield for the same reaction. A dropping mass scenario for the vector mesons (dashed line) leads to a second peak structure at invariant masses of about 650 MeV. The peak around 780 MeV remains practically unchanged since it is dominated by ω mesons decaying outside the nucleus.

With the inclusion of collisional broadening the in-medium peak gets completely washed out (dotted line). The dilepton yield at intermediate masses is about a factor of 2 larger than in the bare mass case. At the two-pion threshold there is a visible discontinuity which results from our neglect of ρ mesons with effective masses below the two-pion mass.

Using the momentum-dependent scalar potential from Eq. (29) we obtain the curves labeled ''momentum-dependent potential'' (dot-dot-dashed lines). The result is very close to the bare mass case as the vector mesons are mainly produced with momenta around 1 GeV for which the potential is zero.

In the lower part of Fig. 16 we show that the effect of a dropping vector-meson mass at a photon energy of 2.2 GeV is qualitatively the same as for 1.5 GeV. The calculation with a momentum-dependent potential gives again a result that is practically the same as for the bare mass case.

In photonuclear reactions vector mesons are in general produced with larger momenta relative to the nuclear medium than in heavy-ion collisions. Since the in-medium spectral functions of the vector mesons are momentum dependent, one might thus observe rather different in-medium effects in both reactions. These, together with additional information from pion-nucleus and proton-nucleus reactions [17], might help to discriminate between different scenarios of medium modifications. Therefore a calculation of all reactions within one model is necessary for a conclusive interpretation of the experimental data. Our BUU transport model provides such a tool.

V. SUMMARY

We have studied e^+e^- production in γC, γCa, and γPb reactions at photon energies of 0.8, 1.5, and 2.2 GeV within a semiclassical transport model. Various contributions were taken into account for dilepton production: Dalitz decays of $\Delta(1232)$, π^0, η, and ω as well as direct dilepton decays of the vectors mesons ρ, ω, and ϕ. We have focused on observable effects of in-medium modifications of the vector mesons ρ and ω.

It was shown that the Bethe-Heitler process which dominates all integrated cross sections for dilepton production can be sufficiently suppressed by appropriate cuts on the lepton momenta. For dilepton invariant masses above 600 MeV the spectrum is dominated by the decays of the vector mesons (ρ,ω,ϕ). A mass shift of these mesons as proposed in Refs. [3,4] leads to a substantial enhancement of the dilepton yield at invariant masses of about 650 MeV by about a factor of 3 and should clearly be visible in experiments that will be carried out at TJNAF [18]. However, a calculation for which we used a linearly momentum-dependent potential for the vector mesons [48] gave practically no effect compared to the bare mass case.

We have stressed the necessity of a simultaneous description of vector-meson production in different nuclear reactions as one probes in-medium properties at different momenta relative to the nuclear medium.

Exemplarily for the case of the ρ and the ω mesons we have discussed the conceptual problems in the treatment of broad resonances in semiclassical transport models. We have presented a prescription that allows one to obtain reasonable results when taking into account in-medium spectral functions.

ACKNOWLEDGMENTS

The authors are grateful for discussions with W. Cassing. This work was supported by DFG and GSI Darmstadt.

[1] C. M. Ko, V. Koch, and G. Q. Li, Annu. Rev. Nucl. Part. Sci. **47**, 505 (1997).
[2] U. Mosel, Annu. Rev. Nucl. Part. Sci. **41**, 29 (1991).
[3] G. E. Brown and M. Rho, Phys. Rev. Lett. **66**, 2720 (1991).
[4] T. Hatsuda and S. Lee, Phys. Rev. C **46**, R34 (1992).
[5] G. Agakichiev *et al.*, Phys. Rev. Lett. **75**, 1272 (1995).
[6] M. A. Mazzoni, Nucl. Phys. **A566**, 95c (1994); M. Masera, *ibid*. **A590**, 93c (1995).
[7] G. Q. Li, C. M. Ko, G. E. Brown, and H. Sorge, Nucl. Phys. **A611**, 539 (1996).
[8] W. Cassing and E. L. Bratkovskaya, Phys. Rep. **308**, 65 (1999).
[9] V. Koch and C. Song, Phys. Rev. C **54**, 1903 (1996).
[10] W. Cassing, E. L. Bratkovskaya, R. Rapp, and J. Wambach, Phys. Rev. C **57**, 916 (1998).
[11] S. Teis, W. Cassing, M. Effenberger, A. Hombach, U. Mosel, and Gy. Wolf, Z. Phys. A **356**, 421 (1997).
[12] M. Effenberger, A. Hombach, S. Teis, and U. Mosel, Nucl. Phys. **A614**, 501 (1997).
[13] B. Anderson, G. Gustafson, and H. Pi, Z. Phys. C **57**, 485 (1993).
[14] M. Effenberger and A. Sibirtsev, Nucl. Phys. **A632**, 99 (1998).
[15] J. Lehr, M. Effenberger, and U. Mosel, nucl-th/9907091.
[16] M. Effenberger, E. L. Bratkovskaya, W. Cassing, and U.

Mosel, Phys. Rev. C **60**, 027601 (1999).
[17] HADES Collaboration, Proposal for a High Acceptance Dielectron Spectrometer, GSI 1994.
[18] P. Bertin *et al.*, CEBAF Proposal No. E94002.
[19] M. Effenberger, A. Hombach, S. Teis, and U. Mosel, Nucl. Phys. **A613**, 353 (1997).
[20] Particle Data Group, Eur. Phys. J. C **3**, 1 (1998).
[21] D. M. Manley and E. M. Saleski, Phys. Rev. D **45**, 4002 (1992).
[22] J. M. Blatt and V. F. Weisskopf, *Theoretical Nuclear Physics* (Wiley, New York, 1952).
[23] J. Geiss, W. Cassing, and C. Greiner, Nucl. Phys. **A644**, 107 (1998).
[24] W. Ehehalt and W. Cassing, Nucl. Phys. **A602**, 449 (1996).
[25] S. Bass *et al.*, Prog. Part. Nucl. Phys. **45**, 225 (1998).
[26] Particle Data Group, R. M. Barnett *et al.*, Phys. Rev. D **50**, 1 (1994).
[27] A. D. Brody *et al.*, Phys. Rev. D **4**, 2693 (1971).
[28] D. M. Manley, R. A. Arndt, Y. Goradia, and V. L. Teplitz, Phys. Rev. D **30**, 904 (1984).
[29] R. S. Longacre and J. Dolbeau, Nucl. Phys. **B122**, 493 (1977).
[30] Ye. S. Golubeva, L. A. Kondratyuk, and W. Cassing, Nucl. Phys. **A625**, 832 (1997).
[31] J. Knoll, nucl-th/9811099.
[32] W. Ehehalt, W. Cassing, A. Engel, and U. Mosel, Phys. Rev. C **47**, 2467 (1993).
[33] W. Peters, M. Post, H. Lenske, S. Leupold, and U. Mosel, Nucl. Phys. **A632**, 109 (1998).
[34] TAPS Collaboration B. Krusche (private communication).
[35] A. Zabrodin *et al.*, Phys. Rev. C **55**, 1617 (1997).
[36] ABBHHM Collaboration, Phys. Rev. **175**, 1669 (1968).
[37] J. Hannappel, Ph.D. thesis, University of Bonn, 1996.
[38] S. Boffı *et al.*, Phys. At. Nucl. **60**, 1193 (1997).
[39] M. Effenberger *et al.* (unpublished).
[40] E. L. Bratkovskaya and W. Cassing, Nucl. Phys. **A619**, 413 (1997).
[41] L. G. Landsberg, Phys. Rep. **128**, 301 (1985).
[42] Gy. Wolf, G. Batko, W. Cassing, U. Mosel, K. Niita, and M. Schäfer, Nucl. Phys. **A517**, 615 (1990).
[43] J. J. Sakurai, *Currents and Mesons* (University of Chicago Press, Chicago, 1969).
[44] H. B. O'Connell, B. C. Pearce, A. W. Thomas, and A. G. Williams, Prog. Part. Nucl. Phys. **39**, 201 (1997).
[45] K. J. Kim and Y. S. Tsai, Phys. Lett. **40B**, 665 (1972); Y. S. Tsai, Rev. Mod. Phys. **46**, 815 (1974).
[46] W. Cassing and S. Juchem, nucl-th/9903070.
[47] Yu. B. Ivanov, J. Knoll, and D. N. Voskresensky, nucl-th/9905028.
[48] L. A. Kondratyuk, A. Sibirtsev, W. Cassing, Ye. S. Golubeva, and M. Effenberger, Phys. Rev. C **58**, 1078 (1998).
[49] A. Baldini, V. Flaminio, W. G. Moorhead, and D. R. O. Morrison, in Numerical Data and Functional Relationships in Science and Technology, edited by H. Schopper, Landolt-Börnstein, New Series, Group I, Vol. 12, Pt. a (Springer-Verlag, Berlin, 1988).